Ariel

Rapid #: -4240250

IP: 128.104.61.85

2

Status	Rapid Code	Branch Name	Start Date
Pending	MYG	Main Library	3/14/2011 12:24:40 PM

CALL #: **QD.M636**

LOCATION: **MYG :: Main Library :: Science Library Journal Collection**

TYPE: Article CC:CCL

JOURNAL TITLE: Mikrochimica acta

USER JOURNAL TITLE: Mikrochimica Acta

MYG CATALOG TITLE: Mikrochimica acta.

ARTICLE TITLE: Use of soft x-rays in microanalysis

ARTICLE AUTHOR: Jean-Louis Pouchou

VOLUME: 13

ISSUE: Supplement

MONTH:

YEAR: 1996

PAGES: 39-60

ISSN: 0026-3672

OCLC #: MYG OCLC #: 1778788

CROSS REFERENCE ID: [TN:1814840][ODYSSEY:216.54.119.76/GZM]

VERIFIED:

BORROWER: **GZM :: Memorial Library**

PATRON:

PATRON ID:

PATRON ADDRESS:

PATRON PHONE:

PATRON FAX:

PATRON E-MAIL:

PATRON DEPT:

PATRON STATUS:

PATRON NOTES:

Mikrochim. Acta [Suppl.] 13, 39–60 (1996)

Use of Soft X-Rays in Microanalysis

Jean-Louis Pouchou

O.N.E.R.A., Department of Materials, 29 Avenue Division Leclerc, F-92320, Châtillon, France

Abstract. The use of soft X-rays in microanalysis is illustrated by several new practical examples, concerning the K lines of the ultra-light elements, and the L lines of medium-Z elements that can be used for near-surface analysis and in situations where eliminating the secondary fluorescence emission is of interest. Some of the specific problems of the soft X-ray field are examined: surface contamination, coating of insulating specimens, line interference, background subtraction, line distortion, mass absorption coefficients.

Key words: soft X-rays, low-energy lines, X-ray microanalysis, electron microprobe, analytical scanning electron microscopy.

In microanalysis, the soft X-ray range can be defined as extending from ~ 1 keV down to ~ 100 eV. This corresponds to photons that could not be detected in the early times of the technique. The wavelength dispersive spectrometers (WDS) of the first generation microprobes could only detect photons above ~ 1.5 keV, i.e. the Al Kα line. Similarly, the first generation of energy dispersive spectrometers (EDS) could not detect photons below the Na Kα line (~ 1 keV). Even when they became detectable, these photons could not be used efficiently for meaningful quantitative analysis because, until the eighties, the approximations in the existing absorption correction models were a limiting factor, as well as the poor knowledge of the values of the mass absorption coefficients, and also the lack of attention paid to the so-called chemical effects (line shift and change of shape due to the chemical bonding).

Nowadays, lines with energies down to ~ 100 eV (the Be K line) can be detected by WDS. The use of multilayer structures as monochromators has strongly improved the X-ray collection efficiency in the low-energy range. However, even in the best excitation conditions, the peak-to-background ratio is not very high (less than 100 for the lightest pure elements), so that the minimum detectable concentration is not very low (a few hundred to a few thousand μg/g, depending on the situation), and the experiments always require more thoughtfulness than at higher energy.

In the case of EDS spectrometry, the new detectors including high-quality semiconductor crystals, improved electronics and ultra-thin atmospheric windows enable measuring elements down to boron (B K line at ~ 185 eV). However, the spectral resolution of these detectors is poor compared to WDS spectrometers (e.g. ~ 70 eV FWHM for the C K line, i.e. at least ten times more than a WD spectrometer

with a lead stearate pseudo-crystal), and the peak-to-background ratio is consequently typically ten times smaller. Hence, one should be aware of the fact that, in spite of the improvements of EDS detectors and software, their potential for fine and accurate analysis will always remain limited in the field of low-energy photons, where spectral interference of elements frequently occurs.

For the ultra-light elements (beryllium to fluorine) there is obviously no other alternative than using soft X-rays. But for other elements, one can wonder if there is some interest in using the low-energy lines (i.e. L lines for medium-Z elements or M lines for heavier elements), since in most current applications these elements can be analyzed without major problem by using the high-energy radiation (i.e. K lines for medium-Z elements or L lines for heavier elements). The aim of this paper is not to give an extensive review of the use of soft X-rays, but to illustrate with practical examples typical situations where the analyst can take advantage of using soft X-rays rather than conventional higher energy lines, and to draw reader's attention to some particular problems with these soft X-rays.

When to Use Soft X-rays?

– To analyze light and ultra-light elements (third and second lines of the periodic table), the soft K lines are the only characteristic lines available.

– To perform analyses with an improved sensitivity to the near-surface region, one has to operate at low accelerating voltage of the electron beam, and to measure the L lines of the medium-Z elements instead of the K lines, or the M lines of the heavier elements instead of the L lines.

– To minimize the effect of secondary emission by fluorescence in multiphase or stratified specimens, one can take advantage of the low fluorescence contribution in the soft X-ray lines.

Use of Soft X-Rays for Surface Analysis

Depth and Efficiency of Excitation

More and more applications of X-ray microanalysis are now concerning surface layers or more generally stratified specimens. When the structure of the stratified specimen is a priori known, measuring the specimen with a high depth resolution is not absolutely necessary. But if the near-surface structure has to be investigated, an improved depth resolution is needed to enable the formulation of reasonable hypotheses. The only way for improving the depth resolution and keeping at the same time a sufficient excitation efficiency is to operate at low accelerating voltage with low-energy characteristic lines. Table 1 illustrates this point in the case of copper. It is interesting to compare the situation obtained at 10 kV for the Cu Kα line (critical energy 8.979 keV) with the situation at 5 kV for the Cu Lα line (critical energy 0.933 keV): these operating conditions give approximately the same mean ionization depth ($\sim 30\,\mu g/cm^2$) and the same maximum ionization depth ($\sim 115\,\mu g/cm^2$), but the peak count rate is ~ 6 times higher and the peak-to-background ratio ~ 8 times higher for the low-energy line. Hence, for the same excited depth, the limit of detection is ~ 7 times better with the Lα line than with Kα. If a smaller analyzed

Table 1. Comparison of the ionization depths[a], peak intensities and peak-to-background ratios for Cu Kα (LiF monochromator) and Cu Lα (TAP monochromator) in copper

Cu Kα	Accelerating voltage (kV)	9.5	10	11	12	13	14	15	
	Overvoltage ratio	1.058	1.114	1.225	1.336	1.448	1.559	1.671	
	Mean ion. depth (μg/cm²)	17	31	53	74	93	113	133	
	Max. ion. depth (μg/cm²)	65	115	200	270	350	425	510	
	Peak (c/s/nA)	0.7	10.4	28	60.4	103.6	154.2	212.1	
	Peak/background ratio	4	27	53	76	116	128	136	
Cu Lα	Accelerating voltage (kV)	1.5	2	2.5	3	3.5	4	4.5	5
	Overvoltage ratio	1.608	2.144	2.680	3.215	3.751	4.287	4.823	5.359
	Mean ion. depth (μg/cm²)	3.7	6.6	10	14	18	22	27	33
	Max. ion. depth (μg/cm²)	14	25	37	49	65	81	98	115
	Peak (c/s/nA)	3.4	9.5	17	27	36	45	57	68
	Peak/background ratio	100	131	148	169	175	176	195	208

[a] Note: the depth from which 90% of the intensity is generated is approximately twice the mean ionization depth.

depth is required, Table 1 shows that a mean ionization depth less than 4 μg/cm² (~4 nm) can be obtained at 1.5 kV in copper with the Cu Lα line. In spite of the low peak counting rate, such an extreme operating condition can be employed in practice, because of the high peak-to-background ratio (~100).

Example of Surface Analysis

The practical interest of soft X-rays can be illustrated by the concrete example of a specimen provided by the N.I.S.T. in view of a round robin test. This specimen was described as a pure chromium layer on a GaAs substrate.

A series of measurements at variable voltage with the usual Kα lines of Cr, Ga and As have been done. Processing the data with the automatic iteration in the program *Strata* seems to give a satisfactory result: as Fig. 1 shows, the computed *k*-ratio curves fit correctly the experimental data (only 0.26% residual absolute deviation) for a Cr layer thickness of 82.7 μg/cm² (i.e. 115 nm assuming 7.19 for the density), and for a substrate composition equal to Ga 49.5 – As 50.5 at.%.

It is almost impossible to get more information with the K lines of the elements declared. However, if one observes the specimen more carefully, the presence of oxygen can be detected. One can measure, at 10 kV for example, a relative intensity greater than 5% of that of an $Y_3Fe_5O_{12}$ conductive oxygen standard. Such a single oxygen measurement does not tell us whether oxygen is incorporated inside the Cr layer, or is in an oxide layer at the surface, or both. To know more, one has to measure the oxygen at several voltages (in particular at lower voltage) and also to generate a Cr signal from a reduced depth, i.e. by use of the Cr Lα line at low voltage. The results are displayed on Fig. 2: at 2.5 kV, the oxygen signal increases strongly, indicating that there is certainly some oxide at the surface. However, the assumption that all the oxygen is in a surface oxide layer does not produce a satisfactory fit of the oxygen data from 2.5 to 15 kV. To get a good global agreement, one has to postulate that some oxygen is also present inside the Cr layer. This is confirmed by measuring

Table 2. Ionization depths, peak intensities and peak-to-background ratios for Cr Lα lines in chromium, for the low voltages used in Fig. 2, (W/Si monochromator, with 2d = 5.9 nm)

Cr Lα	Accelerating voltage (kV)	1.28	1.50	1.80	3.50	5.12
	Overvoltage ratio	2.230	2.613	3.136	6.098	8.920
	Mean ionization depth (nm)	5	6.6	9	27	50
	Max. ionization depth (nm)	18	24	32	93	167
	Peak (c/s/nA)	4.5	6.9	10.2	30	47
	Peak/background ratio	15	17	18	25	29

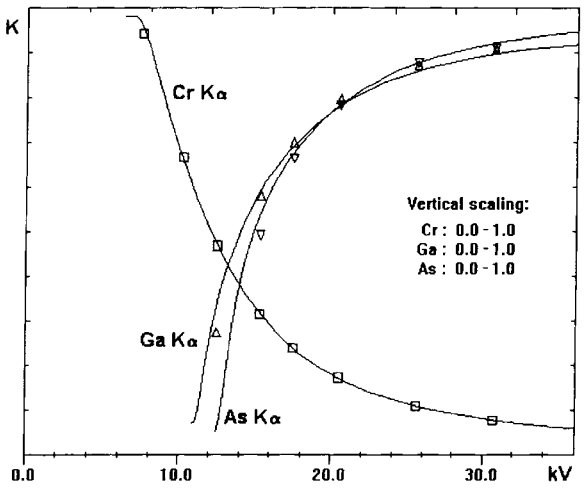

Fig. 1. Comparison of the computed *k*-ratio curves with the experimental data for a Cr layer on a GaAs substrate. K lines for all elements

the Cr Lα line, between ~1.3 kV and ~5 kV. This permits to scan progressively the layer, from near-surface to deeper regions (Table 2). On Fig. 2, the observed decrease of the Cr Lα data at very low voltage confirms the assumption of a surface oxide layer, while the level of the "plateau", near 4 kV, agrees with the hypothesis of incorporated oxygen. Finally, the curves of Fig. 2 are obtained for the following specimen description: a GaAs substrate, covered by a 87 μg/cm^2 layer (i.e. 121 nm assuming 7.19 for the density) of Cr containing 3.2 at.% oxygen, and with a surface oxide layer of 1.25 μg/cm^2 (i.e. 25 nm assuming Cr_2O_3 with a density equal to 5).

Use of Soft X-Rays to Minimize Fluorescence Effects

In the Cr Kα *k*-ratio curve of the previous example (Fig. 1), it can be noted that the value of the narrow plateau computed at very low overvoltage for a pure chromium layer is lower than 100%. This is the effect of the secondary emission by fluorescence, the contribution of which to the total emission is less for the thin Cr film than for a bulk reference.

Fluorescence is probably the most worrying effect for high-energy lines, because it may produce not only quantitative errors, but also wrong qualitative interpretation of the measurements, since the volume concerned by fluorescence is much greater than the primary volume excited by the incident electrons, so that a radiation

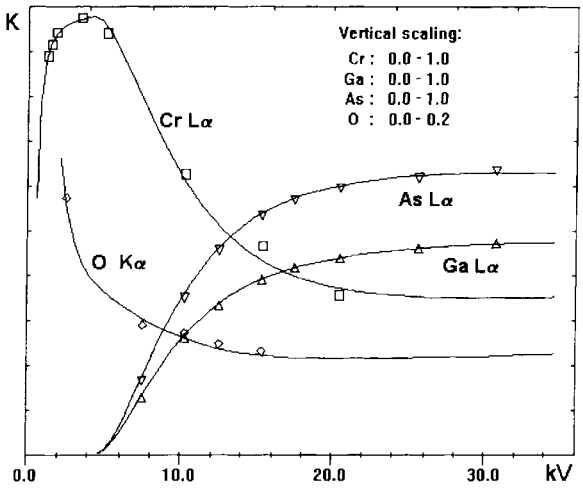

Fig. 2. Comparison of the computed *k*-ratio curves with the experimental data for a Cr layer on a GaAs substrate. L lines for all elements, except oxygen

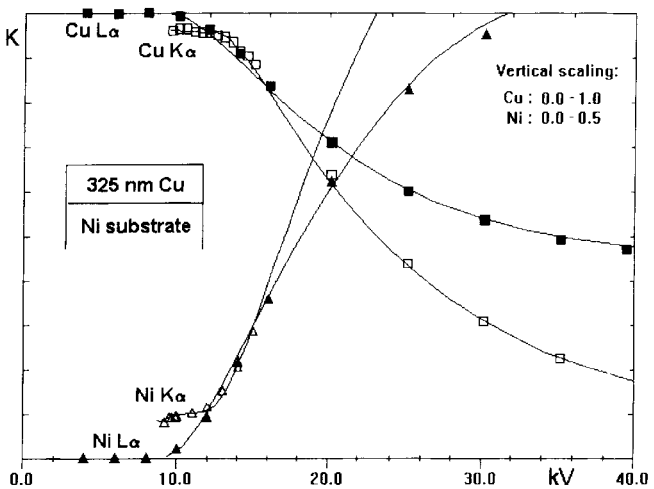

Fig. 3. *k*-ratio vs. accelerating voltage for a 325 nm Cu layer on Ni substrate. The K lines (open symbols) show the effect of fluorescence, negligible for the L lines (close symbols). Curves modeled with *Strata*

can be excited far away from the point of electron impact. This paragraph illustrates this point, and shows that the problem can be eliminated with soft X rays.

Fluorescence in Stratified Specimens

The importance of the fluorescence for high energy lines can be appreciated easily on Fig. 3, in the simple case of a Cu layer (325 nm) on a Ni substrate. In that case, the Ni Kα line is excited both by the continuum and by the Cu Kβ line, whereas the Cu Kα line is excited by the continuum only. Provided that the surface cleanliness is the same for the Cu layer and for the Cu standard (the best is to evaporate simultaneously the Cu layer onto the bulk Cu standard), one can measure at low overvoltage that the Cu Kα plateau is not at 100%, but near 96.5% at 10 kV. At the same time, the Ni Kα *k*-ratios are not equal to zero below the threshold for primary substrate excitation ($\sim$ 12 kV), but are near 4.5% at 10 kV. The interesting point to observe on Fig. 3 is that the use of the Lα lines, for which the fluorescence yield is much lower,

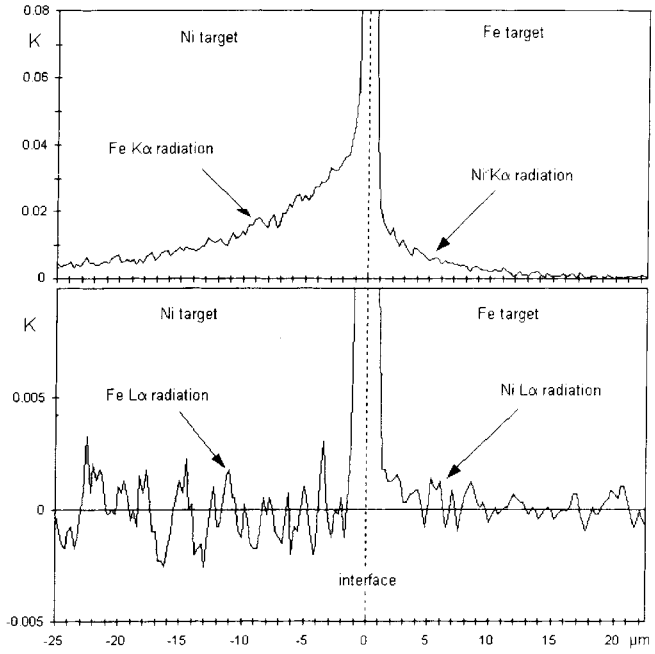

Fig. 4. Fe and Ni *k*-ratios measured with K and L linss on each side of a Ni–Fe interface. The fluorescence is eliminated by use of L lines

eliminates completely (in the limits of the experimental accuracy) this disturbing effect: for example, the Ni Lα *k*-ratios mesasured from 4 kV to 8 kV are ranging between 0.01% and 0.02%.

This example of stratified specimens corresponds to a well-defined geometry, for which calculations have been developed [1] and incorporated in some available computer programs (e.g. *Strata, Multifilm*). But the problem of fluorescence may also be crucial in many other current situations where the analysis is performed not far from an interface (e.g. diffusion near an interface, analysis of particles smaller than a few tens of µm).

Lateral Fluorescence Near Interfaces

The example of Fig. 4 illustrates the lateral fluorescence in the vicinity of an interface, in the case of a Ni-Fe couple on which line scans across the interface have been performed. To avoid absorption artifacts, the plane of the interface was located in the vertical plane defined by the electron beam and the direction of the spectrometer. Both the Kα and the Lα lines of Fe and Ni have been measured. To obtain primary excitation volumes having approximately the same dimensions, the voltage was set to 15 kV for the K lines and 12 kV for the L lines. The difference in the behavior of both elements, on each side of the interface, is due to the fact that Ni K is only excited by the continuum, whereas Fe K is excited by continuum and by the Ni Kα and Kβ lines. Figure 4 shows clearly that the fluorescence is much stronger on the Ni side (for the Fe Kα radiation) than on the Fe side (for the Ni Kα radiation): respectively 3.3% and 1% at 3 µm of the interface, 1.4% and 0.2% at 10 µm, 0.7% and 0.03% at 20 µm.

On the other hand, when the soft Lα lines are used (bottom of Fig. 4), one can observe that the contribution of the fluorescence is almost undetectable. Hence,

this shows again that the analyst can take advantage of using soft lines instead of the usual ones in order to eliminate strong fluorescence effects and to determine more easily if an element is actually present or not in a given phase, particle, or layer.

Particular Problems of Line Shape Distortion

Since the effort made in the beginning of the eighties to quantify the ultra-light elements, it has been clearly shown that the characteristic emission bands of these elements were suffering the so-called "chemical effects", i.e. the spectral distribution of the intensity was dependent on the nature of the compound. Generally speaking, the stronger the chemical bonding, the narrower the line of the ultra-light element. Although some basic work is still needed in this field [2], the experience has shown that in most situations (except the Ni and Co borides [3]) the ultra-light elements can be properly analyzed quantitatively by WDS [4], provided that peak areas are used to form the relative intensities, either directly [5] or through the so-called APF (area-to-peak factors) [6]. Recent WDS software, such as the programs distributed by *CAMECA* and *SAMx*, include automatic area acquisition by scanning the spectrometers. In addition, the latter also enables to combine conventional peak measurements with APF factors.

For other soft X-rays, such as the Lα lines of the 3d transition elements, other phenomena may appear, i.e. important changes in the Lα generation and in the self-absorption, depending on the chemical state of the transition atom [7]. Understanding these phenomena is necessary to avoid serious errors in using these soft lines. This is the objective of this paragraph.

In the examples of the previous paragraphs, there was no danger in using the Lα lines of transition elements Cr, Fe and Ni, because these elements were pure (or almost pure) in the specimens as well as in the standards. But when such a transition atom is chemically bonded with another element in a compound, the partial filling of the 3d electron band modifies both the generated Lα intensity (because Lα results from a 3d–2p transition, so that its intensity increases with the 3d population), and also its self-absorption (because the filling of the 3d band attenuates the anomalous Lα absorption resonance corresponding to the possible 2p–3d promotion of electrons by the most energetic photons of the Lα line). This paragraph aims to clarify some observations about the Ni Lα line, which could be interpreted as chemical effects (i.e. the image of strong changes in the electron distribution of the 3d band), but which actually result mainly from an absorption effect, the attenuation of the Ni Lα resonant absorption when the nickel is alloyed.

If one compares the spectra acquired at 30 kV on pure Ni and on the NiAl compound, in the region of the Ni L lines (Fig. 5), it seems that the Ni Lα line of the compound is shifted towards the high energies by ~ 0.6 eV. Incidentally, it can be observed that the high-energy tail of the Ni Lα line appears weaker in the compound than in the pure metal. Actually, the apparent shift is not due to a chemical effect, as demonstrated by Fig. 6: if the same spectra are recorded at 3 kV, where the absorption is very weak, the Lα line has almost the same position and the same shape in NiAl as in pure Ni (only a slight difference in the high- and low-enery tails can be observed). This demonstrates clearly that the effect observed at high voltage is not

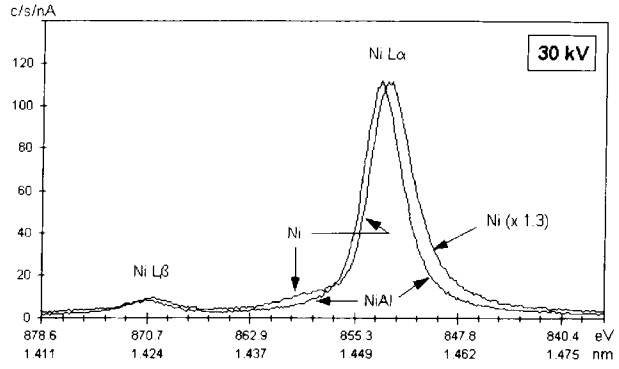

Fig. 5. Ni L spectra from Ni and NiAl at 30 kV. WDS spectrometer with TAP monochromator

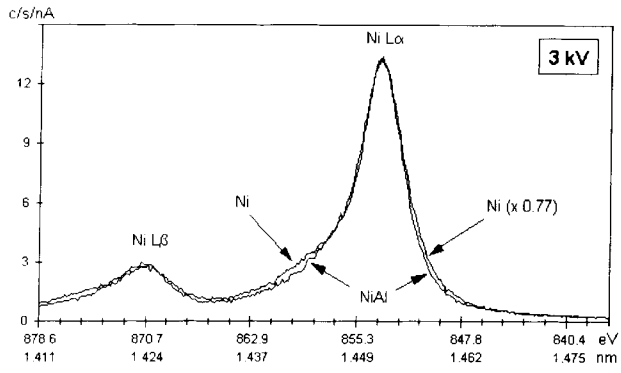

Fig. 6. Ni L spectra from Ni and NiAl at 3 kV. WDS spectrometer with TAP monochromator

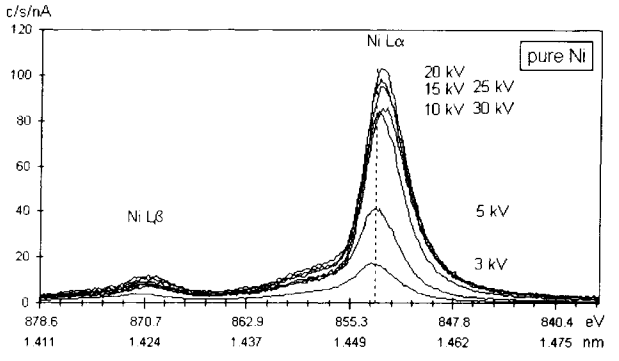

Fig. 7. Evolution of the Ni L spectrum with accelerating voltage in pure Ni

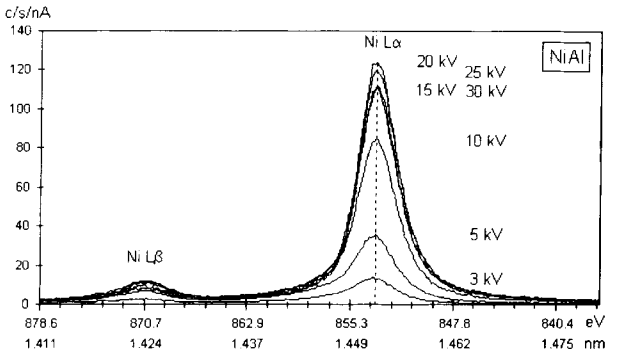

Fig. 8. Evolution of the Ni L spectrum with accelerating voltage in NiAl

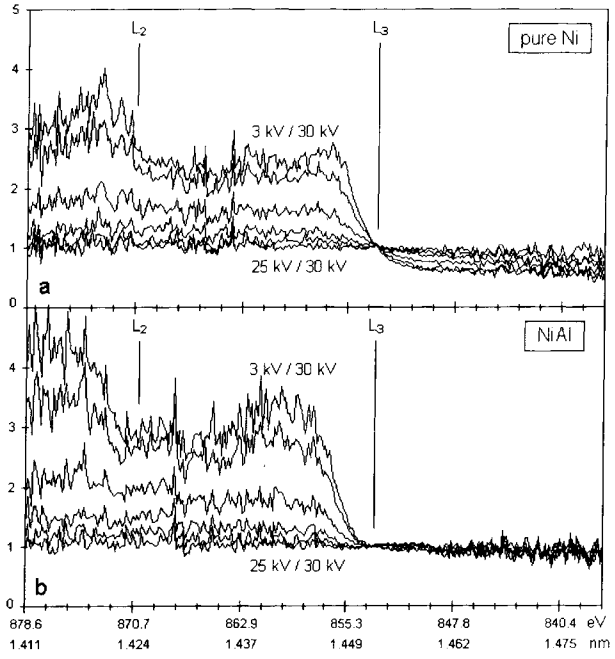

Fig. 9. Ratio of Ni L spectra to the 30 kV spectrum. **a** Case of pure Ni, **b** case of NiAl

a real chemical effect, but an absorption effect due to the attenuation of the resonant self-absorption in NiAl compared to pure Ni.

If one compares on Fig. 7 (case of Ni) and Fig. 8 (case of NiAl) the variations of the NiLα spectra with the accelerating voltage, one can see that the depression in the Ni spectrum near the L_3 edge (854 eV according to [8]) almost disappears in the NiAl spectrum. Similar measurements on the Ni_3Al compound (not presented here) show an intermediate behavior between Ni and NiAl.

By ratioing the spectra recorded at every voltage to the 30 kV spectrum (taken as reference because it has the best counting statistics), one obtains the graphs of Fig. 9a and 9b, which show clearly the actual positions of the L_2 and L_3 absorption edges (the positions marked on the graph are from [8]). By dividing the 3-to-30 kV NiAl ratio (which represents the maximum absorption effect) by the corresponding ratio for pure Ni, one gets a graph (Fig. 10) which enhances the difference in the behavior of pure and bonded Ni atoms, and shows the energy of the resonant absorption for the Ni Lα line and incidentally for the Ni Lβ line.

The fact that the 3d–2p transition rate and the L self-absorption coefficient vary with the chemical state in the 3d transition elements is a strong limitation for the use of their L lines in routine applications of quantitative microanalysis. However, these lines can be used efficiently in particular cases of thin film analysis: when the transition element is almost pure in a given layer, or, in the opposed situation, when a standard with a similar composition is available (for example a thick film, with a composition previously measured with the K lines). Whatever the situation, the effective value of the self-absorption coefficient of the L line in the transition element is needed.

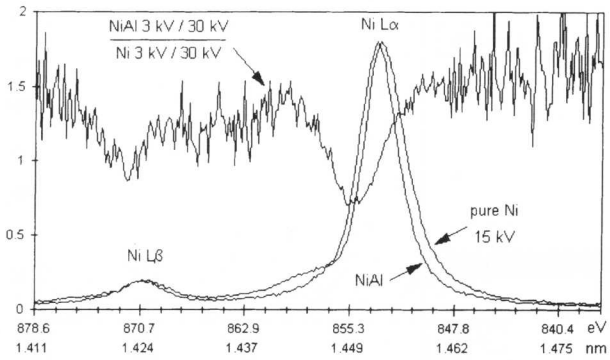

Fig. 10. Ratio of (3 kV/30 kV) NiAl curve (Fig. 9b) to the corresponding Ni curve (Fig. 9a). The observed resonant absorption is on the high-energy side of Ni L lines

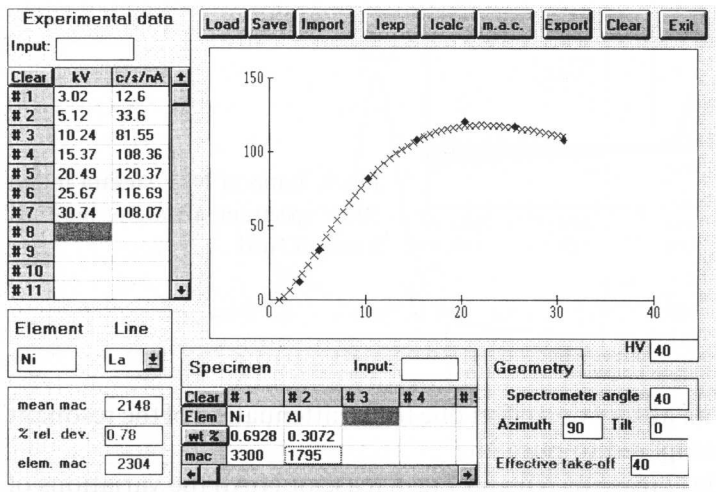

Fig. 11. Determination of the mass absorption of Ni Lα by Ni atoms in NiAl (*XMAC* program)

The Determination of Soft X-Ray Absorption Coefficients

Accurate $\phi(\rho z)$ models have been developed during the last decade for quantitative analysis, but none of them is able to produce good results without a set of reliable values for the X-ray mass absorption coefficients.

Frequently, in the soft X-ray field, one has the problem that an analyzed line is close to an absorption edge, or suffers some anomalies as in the previous example. Consequently, the absorption coefficient may be quite uncertain. An efficient method for determining an absorption coefficient is to measure and process the variation of the line intensity emerging from a known composition as a function of the accelerating voltage. The advantage and the principle of the method, initially based on the $PAP\phi(\rho z)$ model, have already been described [9]. Recently, a new software (*XMAC*) based on the *XPP* model has been developed by the author for the *SAMx* user's group.

An application of this program, in the case of the Ni Lα line in NiAl, is shown on Fig. 11. In this typical example, the absorption coefficient of Ni Lα in Al is supposed to be known exactly (1795 cm^2/g according to [10]). The self-absorption of Ni Lα by Ni atoms bonded with Al has to be determined. It should be noted that the value of 3300 displayed in the "Specimen" box is the indicative value of the self-absorption

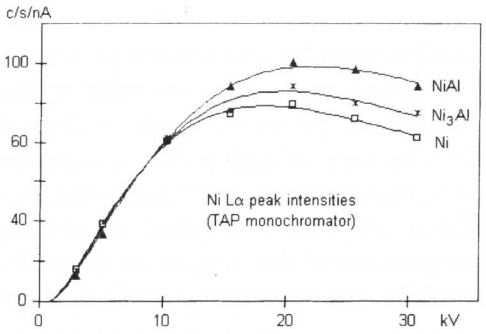

Fig. 12. Variation of the Ni Lα peak intensity vs. accelerating voltage emerging from pure Ni, Ni_3Al and NiAl

proposed by the program for pure Ni atoms. For bonded Ni atoms, one expects a lower value. The emerging intensity is measured at the Ni Lα peak maximum from ~3 kV to ~30 kV. An automatic iterative procedure searches the value of the mass absorption coefficient for which the computed intensity variation (the series of crosses) fits at best the experimental data. The resulting absorption coefficient of Ni Lα in Ni bonded with one Al atom is displayed at the lower-left corner of Fig. 11. This result (2304 cm^2/g) is significantly lower than the value 3300 for pure Ni. It should be mentioned that, if area measurements are performed instead of peak measurements, the resulting value of the effective self-absorption coefficient is slightly higher (2575 cm^2/g), because of the greater contribution of the resonant absorption). In the case of the Ni_3Al compound, a similar measurement of the peak intensity versus the accelerating voltage has given 2850 cm^2/g, i.e. an intermediate value between pure Ni and NiAl. Hence, the attenuation of the resonant absorption near the Ni L_3 energy, when the concentration of Al atoms increases, is responsible for the apparent shift of the Ni Lα line, because the absorption is stronger on the high-energy side than on the low-energy side of the line.

Finally, if the absolute emerging intensity curves for Ni, Ni_3Al and NiAl are plotted on the same graph (Fig. 12), one can paradoxically observe at medium and high accelerating voltages that, the lower the concentration of nickel, the higher the emerging intensity of its Lα line! This illustrates that in the field of soft X-rays, mainly for the transition elements, the analyst should always keep in mind that unusual effects may appear, and that he should approach very carefully any new problem.

The Problem of Surface Contamination

When soft X-rays in general and ultra-light elements in particular have to be analyzed, the polishing and rinsing of the specimens and standards have to be done with a lot of care. Any significant deterioration of the target under the beam should also be avoided. The most frequent problem is the carbon contamination due to the cracking of the residual organic molecules of the vacuum, and also the contamination coming from the target itself.

Case of Electron Microprobes

In the electron microprobes, the problem is solved by combining an oxygen- (or air-) jet with a N_2-cooled trap. Such a system is able, generally after typically 2 or

3 minutes, to eliminate the absorbed carbon from the region of the surface bombarded by the electrons. The most recent microprobe automation programs (*XMAS* for example) allow the user to define a decontamination time prior to the measurement at each point. Future versions should probably apply statistical criteria to the variation of the carbon signal versus time at each point, in order to determine and manage automatically the decontamination process. One should also be aware that some materials (e.g. zirconium) are highly sensitive to surface oxidation and may react under the beam in the presence of the oxygen- or air-jet. In such cases, an hydrogen-jet can be used successfully, although the time required for decontamination is longer [11].

Case of Scanning Electron Microscopes

Most often, the scanning electron microscopes don't have any anticontamination device. The main reason is that, contrary to the electron microprobes, these instruments have to be operated in widely variable conditions of working distance, stage position and tilt, so that the attachment of a fine capillary tube near the specimen surface, very close to the beam, is not easy. The consequence is that the carbon contamination is important, even in the microscopes equipped with a turbo-molecular pump, since most of the contamination comes from the primary rotary pump.

On Figs. 13 and 14, the EDS spectra recorded with a *Kevex Super Quantum* detector illustrate how the carbon signal measured on a Fe_3C specimen varies with the counting conditions. All the spectra correspond to a total counting time of 1000

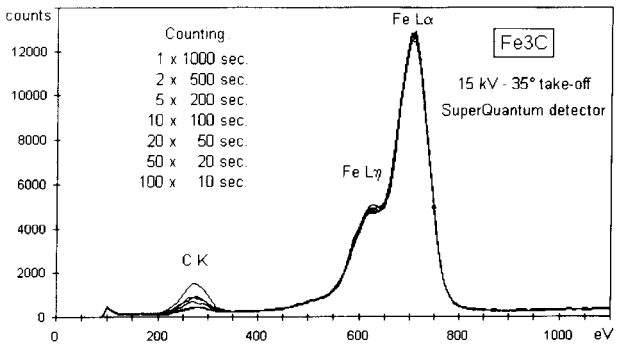

Fig. 13. Low-energy portion of Fe_3C energy dispersive spectra for variable counting time per point

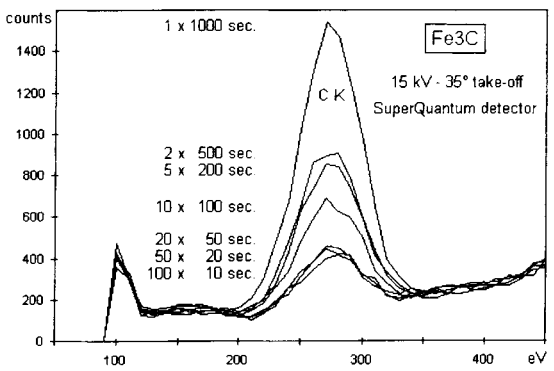

Fig. 14. Enlarged view of the carbon spectra of Fig. 13

Table 3. Influence of carbon contamination on the result of standardless carbon analysis in Fe_3C (6.68 wt.% nominal). *Quantex*$^+$ program with *XPP* model

Time per point (seconds)	10	20	50	100	200	500	1000
wt. % carbon (*XPP* procedure)	1.56	6.35	6.47	10.84	13.68	14.52	22.77

seconds, achieved either by counting once on a single point, or by summing N spectra acquired on N different points during 1000/N seconds. The first observation from Fig. 13 is that the carbon peak has a low intensity compared to the Fe L lines. This is due to the strong absorption of the C K line both in Fe and in the detector window (the main constituent of the *SuperQuantum* window is boron, which absorbs the C K line with a maximum efficiency). This low intensity justifies that long counting times have to be used to get a statistically well-defined peak for ultra-light elements. Zooming over the C K peak (Fig. 14) shows the effect of the contamination. For individual counting periods of 10, 20 and 50 seconds per point, the C K spectra are almost identical. But for longer periods, the "apparent" carbon signal increases strongly (more than threefold for 1000 s.). In the present example, processing the spectra with the standardless *Quantex+/XPP* procedure [12] leads to a carbon content in good agreement with Fe_3C (see Table 3) only for the short counting periods (less or equal 50 s). By applying *Strata* to the high carbon signal obtained for 1000 seconds per point, one obtains $\sim 15\,\mu g/cm^2$ carbon (i.e. ~ 75 nm) due to the contamination on the specimen surface.

It should not be forgotten that the contamination by carbon is a problem not only in the case of the carbon measurement, but also for the measurement of other soft X-rays (mainly the nitrogen line, which is the most strongly absorbed by carbon). For example, to give an order of magnitude, one can calculate with *Strata* that, at 10 kV and 35° take-off, the presence of 75 nm carbon at the surface of a boron nitride produces a relative loss of intensity of 11% for the B K line and 46% for the N K line. At 5 kV, where the losses of direct ionization becomes significant, these values are respectively 23% and 54%. Obviously, this is a strong source of error in EDS standardless analysis, since there is in that case no check of the result, because of the necessary normalization of the concentrations.

The Problem of Coating the Insulating Targets

In many cases, ultra-light elements have to be analyzed in insulating specimens (oxides, nitrides, ...). The conventional procedure consists in depositing simultaneously the same conductive coating on the specimen and on the standards, considering that the influence of the coating on the intensity loss for a given X-ray line is the same for all targets. To minimize the loss of intensity due to the coating, most people evaporate a light element, carbon, except when this element is present inside the specimen.

The analysis of insulating specimens is actually a serious source of problems. The main question is to know if the electrical field which subsists inside the specimen [13], in spite of the conductive coating, produces significant changes in the $\phi(\rho z)$

functions, able to modify strongly the X-ray emission, or not. To try to answer this question, it is essential to eliminate all the sources of errors, which would lead to erroneous conclusions. This paragraph comments a few aspects that need to be examined with care.

Influence of the Coating on the Emerging Intensity

The first point is that it may be a wrong assumption to consider that the influence of a given coating is the same for a given line, whatever the nature of the target. Actually, this is completely false in all the situations where the mass absorption coefficient of the line of interest is very high in the target and lower in the coating, for example when boron is analyzed in a Si-rich target coated with carbon or gold (μ/ρ B K in C ~ 6750; (μ/ρ B K in Au ~ 10400; μ/ρ B K in Si ~ 80000). In such situations, the emission of the coated target can be higher than that of the same, but uncoated, target (hypothetically conductive). For example, in the case of a borosilicate glass supposed to contain 10 wt. % B_2O_3 in SiO_2, one can calculate with *Strata* the values reported in Table 4. They show that there is a range of coating thickness (up to ~150 nm for C and ~15 nm for Au, i.e. up to ~30 µg/cm^2 for both coating materials) that produce an emission enhancement.

This surprising effect can be simply explained on the basis of the $\phi(\rho z)$ model. The intensity emerging from an homogeneous specimen is proportional to the integral of $\phi(\rho z)\cdot\exp(-\chi\cdot\rho z)\cdot d\rho z$, from $\rho z = 0$ to infinity. For the coated specimen, with the approximation that the $\phi(\rho z)$ function is not significantly modified, the emerging intensity is the integral of $\phi(\rho z)\cdot\exp[-\chi\cdot(\rho z-\rho z_c)]\cdot d\rho z$ from $\rho z = \rho z_c$ to infinity, multiplied by the factor $\exp(-\chi_c\cdot\rho z_c)$ to account for the absorption by the coating (mass thickness ρz_c and absorption factor χ_c for the line of interest). In the case of the borosilicate glass, the absorption of the B K line is very strong in the target, so that only the initial part of the $\phi(\rho z)$ function at 10 kV has actually some effect on the result (Fig. 15). For a simple calculation "by hand", one can take the approximation that in this region the slope S of $\phi(\rho z)$ is constant, so that the interesting part of $\phi(\rho z)$ can be expressed as $\phi(0)+S\cdot\rho z$. Here, $\phi(0)$ is so-called surface ionization.

With this approximation, the calculation of the intensity for the uncoated specimen gives

$$I_{\text{uncoated}} \sim [\phi(0) + S/\chi]/\chi$$

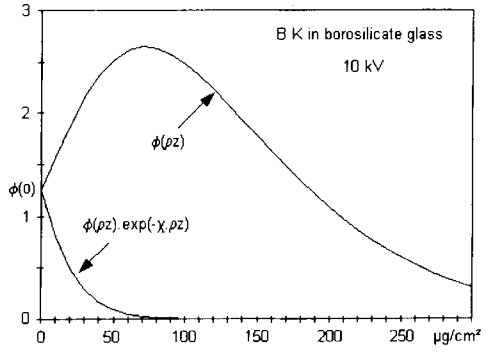

Fig. 15. Depth distributions of the generated and emerging B K intensities for a borosilicate glass at 10 kV. (*XPP* model, 40° take-off angle)

Table 4. Computed relative change in the B K intensity emerging from a borosilicate glass coated with carbon or gold, compared to the uncoated target (supposed to be conductive). 10 kV, 40° take-off angle, *Strata* with *XPP* model

C coating thickness (nm)	5	10	20	40	80	120	160
Relative change of intensity (%)	+0.5	+0.9	+1.7	+3	+3.9	+2.7	−0.4
Au coating thickness (nm)	1	2	4	8	12	16	
Relative change of intensity (%)	+3.3	+6	+9.9	+11	+6.6	−1.9	

Table 5. Result of the analysis of an olivine coated with carbon (4.5 μg/cm^2). *Strata* program. All elements analyzed

Element	O	Mg	Si	Fe	Total
wt. %	48.1	29.1	19.3	9.1	105.6

For the coated specimen, one obtains

$$I_{\text{coated}} \sim \exp(-\chi_c \cdot \rho z_c) \cdot [\phi(0) + S(1/\chi + \rho z_c)]/\chi$$

Hence, if the quantify $1 + S \cdot \rho z_c/[\phi(0) + S/\chi]$ is greater than $1/\exp(-\chi_c \cdot \rho z_c)$, then I_{coated} is greater than I_{uncoated}. This condition can be realized only by the combination of a high absorption factor χ in the specimen, a lower absorption factor χ_c in the coating, and a moderate thickness of the coating. The higher effect reported in Table 4 for the gold coating than for the carbon coating results from the higher electron scattering power of gold, which increases the slope S.

Nature of the Coating

It is not sure that coating the insulating specimens (and mainly oxides) with carbon is the best procedure to adopt. We had already briefly mentioned [14], that we were obtaining better quantitative analyses for a SiO_2 specimen after coating it with aluminium than with carbon. New comparisons have been made, in the case of a couple of olivine specimens (having slightly different MgO and FeO fractions), the one coated with evaporated carbon, the other one with sputtered gold. The oxygen is analyzed with respect to a conductive $Y_3Fe_5O_{12}$ standard (uncoated), the other elements with pure standards. The program *Strata* is employed for the data reduction.

For the C-coated specimen (4.5 μg/cm^2 carbon, i.e. 22.5 nm assuming that the density equals 2), all the elements being analyzed at 10, 15, 20 and 25 kV, one obtains before normalization the unsatisfactory results of Table 5, with the sum of the concentrations close to 105%. It can be mentioned that a bad sum is also found if, instead of processing all the voltages together, one considers only the data at the lowest or at the highest voltage.

If oxygen is not measured, but obtained by stoichiometry, one gets the results of Table 6, showing that only the oxygen result changes significantly, and that the measurement of the other elements leads to a correct sum, close to 100%.

Table 6. Same as Table 5, but with oxygen determined by stoichiometry

Element	O	Mg	Si	Fe	Total
wt. %	43.6	28.7	19.4	9.1	100.8

Table 7. Results of the results of an olivine coated with gold (17.2 μg/cm^2). *Strata* program. All elements analyzed

Element	O	Mg	Si	Fe	Total
wt. %	43.7	26.2	19.1	11.9	100.9

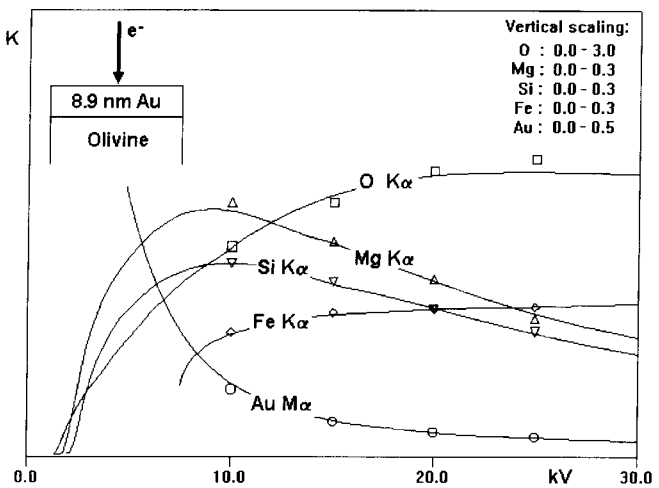

Fig. 16. Display of *Strata* relative intensity curves vs. accelerating voltage for a gold-coated olivine (~8.9 nm gold)

On the opposite, for the Au-coated specimen (17.2 μg/cm^2 Au, i.e. 8.9 nm assuming the nominal density), the results of Table 7 show that there is no problem with the sum when all the elements are analyzed. The *k*-ratio curves drawn for the specimen description resulting from the iterative procedure of *Strata* fit satisfactorily the experimental data (Fig. 16).

One of the reasons that could explain the excess of oxygen found for a carbon-coated specimen is that some oxygen could be incorporated into the coating during the carbon evaporation. This possibility has been checked by evaporating a similar carbon film on one half of a clean nickel substrate (the other half was hidden during the evaporation in order to deduce the natural amount of oxygen at the surface of nickel). An oxygen concentration of ~4% was actually found in the carbon film. However, such a concentration is quite insufficient to explain the excess of oxygen reported in Table 5: when 4% oxygen is incorporated into the 22.5 nm carbon layer, the result given by *Strata* for the oxygen in olivine decreases only slightly (47.9% instead of 48.1%). Hence, one has to admit that an evaporated carbon film with a thickness in the range of ~20 nm might not be conductive enough to ensure an efficient electrical grounding of the specimen surface. On the opposite, we have the feeling that a thin gold coating (a few nanometers thick) made by sputtering (to avoid

Table 8. Some first order lines interfering with ultra-light elements

Analyzed line	Energy (eV)	Interfering lines
Be K	109	Sr Mζ
B K	183	Nb Mζ
C K	277	K Ll, η Mo Mζ
N K	392	Sc Lα, β Ti Ll Sn Mζ
O K	525	V Lα, β Cr Lη Mn Ll

the formation of islets and to obtain a better adherence to the substrate) might be the best choice for the analysis of insulating materials.

Line Interference in WDS Spectrometry

It is frequent in the soft X-ray region that the characteristic line of interest interferes with some lines of other elements. It is easy to eliminate the interference with high-order lines, by selecting an appropriate band width for the pulse height analyzer (PHA). It can be noted too that there is an advantage in using multilayer monochromators, which are optimized to strongly attenuate the 3n orders of diffraction. Hence, the problem of interference actually subsists for the first order lines. Table 8 gives a few examples of such lines interfering with the ultra-light elements. Fig. 17 shows the example of the interference of the oxygen K line with the chromium L lines.

The most recent computer programs for electron microprobes include the automatic processing of the interference. To make this possible, one should perform a preliminary measurement of an "interference standard" that emits the same interfering line as in the specimen (same wavelength and shape). With this assumption, two different approaches can be used:

Peak Acquisition

If the line of interest is not subject to detectable shape alterations by chemical effects, the intensity I_{peak} of this line can be measured at peak maximum. The intensity I_{int} of the "interference standard" is measured at the same position. In the *CAMECA* or in the *SAMx* microprobe automation and data processing software, the interference is taken into account at each loop of the iteration procedure which leads from the experimental relative intensities to "corrected" mass concentrations. At every loop, the concentration C_{int} of the interfering element (measured with another non-interfering line) is evaluated. Using this particular concentration and the concentrations of the other elements presents in the specimen, the contribution $C_{int} * I_{int} * ZAF$ of the interfering line to the line of interest in the specimen is computed by applying the atomic number, absorption and fluorescence corrections through the correction procedure (*PAP*, *XPP* or other).

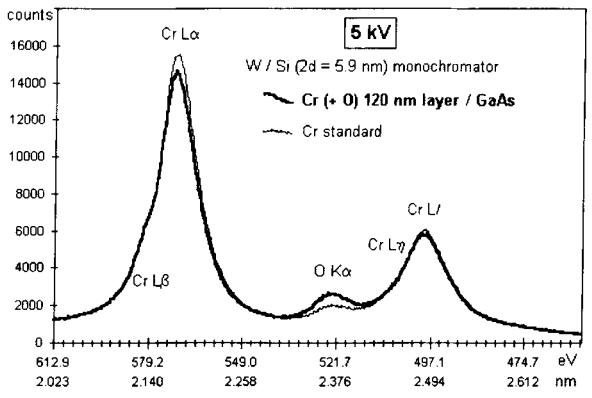

Fig. 17. Interference of the oxygen K line with the Cr L lines (W/Si multilayer monochromator 2d = 5.9 nm)

Integral Acquisition

In the software produced by *SAMx*, an integral mode is additionally available. In this mode, the line of interest, as well as the interfering line, are measured by scanning the spectrometer over a wide spectral region. This allows to apply the interference processing to those situations where the line of interest is shifted and/or distorted by chemical effects. Obviously, the "interfering standard" is also acquired in integral mode. Then, as in the previous mode, its intensity is incorporated in the correction procedure. It should be pointed out that in the present version of the software, the absorption coefficient applied to all the interfering band is that of the interfering line. This can be a limitation if a strong absorption jump is present in the integration band. For such cases, the software should be further improved by allocating the proper absorption coefficient to each channel of the spectrum.

Case of Stratified Specimens

In the case of stratified specimens, there is presently no program able to do the same as for bulk specimens (except in the case of a surface layer thicker than the analyzed depth, where one of the programs mentioned previously may be used). In the example of the Cr layer on GaAs, previously presented on Fig. 2 and Fig. 17, the oxygen contamination had to be determined. The only way to get the oxygen peak coming from the specimen was to deduce from the specimen spectrum the spectrum of a pure chromium standard, after scaling it down to superimpose the Cr Lα lines. The general problem with the analysis of oxygen is that it is almost impossible to get a standard with no oxygen or oxide at the surface. In the present case (Fig. 17), the spectrum of the standard was exhibiting an oxygen peak that could correspond to ~ 1 nm Cr_2O_3 oxide at the surface.

Background Subtraction in Low-Energy EDS Spectra

Bremsstrahlung and Actual Background

To succeed in performing quantitative analysis with soft X rays, one has firstly to overcome the problem of the background subtraction. Two different methods are

available in the commercial programs: the quickest one is to apply over the spectrum a "top hat" numerical filter; the other one is to model the background theoretically. In the case of the *Kevex* system used in our laboratory, the filtering the low energy region numerically leads at the end to poor quantitative results. For example, in the case of SiC standardless analysis, the carbon concentration is overestimated by more than 20% relative.

If the theoretical background modeling is applied, the *Quantex* +/*XPP* procedure actually computes the emerging intensity of the "bremsstrahlung" radiation, taking into account its absorption inside the specimen and through the *Super Quantum* detector window. The problem is that in the low-energy region, even when the "optimize" option of the background computation is selected [15], the computed "bremsstrahlung" does not fit the actual background (Fig. 18), which contains other contributions, i.e. mainly the electronic noise of the detector, and a "spur" [16] with a tail extending to ~500 eV due to incomplete charge collection. This "spur" depends on the shape and on the intensity of the spectrum. It is obvious on the example of Fig. 18 that below the C K line, the predicted "bremsstrahlung" intensity is almost zero (because of the absorption), whereas the actual background represents at least 10% of the peak height. To overcome the problem, the simplest way is to use a standard emitting a spectrum similar to the specimen's one, but without any line in the region of interest. In the present example, the best choice is to record a spectrum on pure Si. Obviously, this spectrum (Fig. 19) exhibits the same problem as the SiC spectrum: its computed "bremsstrahlung" is lower than its actual background. Additionally, the Si reference spectrum exhibits small carbon and oxygen peaks corresponding respectively to carbon contamination and native oxide. After subtracting the "bremsstrahlung" from the Si spectrum and erasing all the channels above ~600 eV, one gets experimentally the dotted region (Fig. 19), consisting

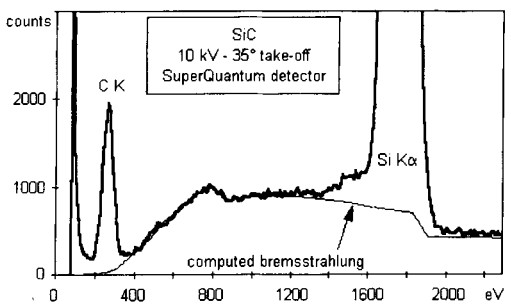

Fig. 18. Low-energy region of an EDS spectrum from SiC and from the computed bremsstrahlung

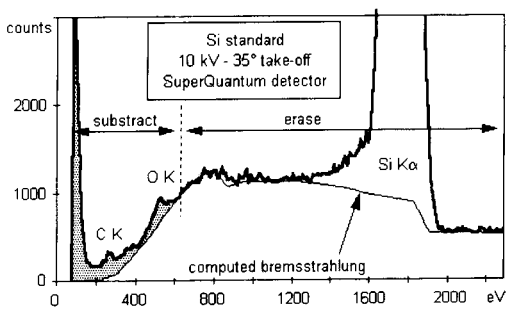

Fig. 19. Low-energy region of an EDS spectrum from a Si standard. The dotted region is the "spur"

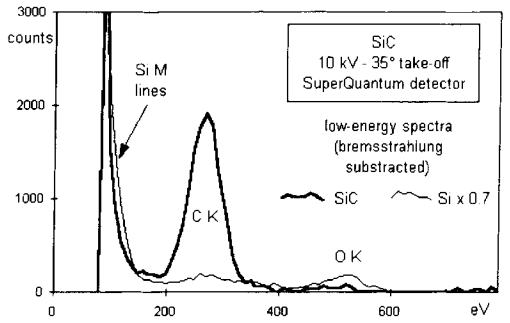

Fig. 20. "Spur" contribution (obtained from Fig. 19), to be subtracted from SiC spectrum

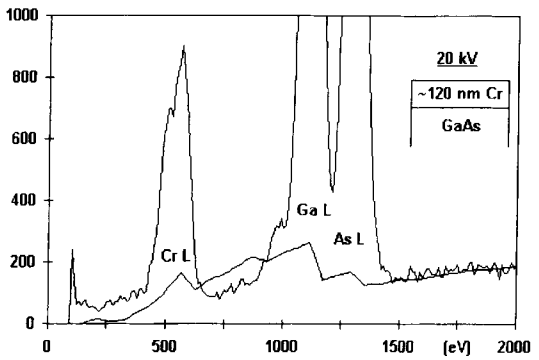

Fig. 21. Comparison of the actual low-energy EDS background for a Cr/GaAs stratified specimen with the background modeled in *Quantex*$^+$*XPP* assuming an homogeneous specimen

mainly of the "spur", plus the electronic noise, the surface imperfections and, in this particular case, some contribution of the Si L lines. The final step of the processing is to deduce from the SiC the proper fraction of this dotted region. Since the "spur" is the main constituent, one can take the ratio of the total number of counts in the SiC spectrum to the Si spectrum, i.e. ~ 70%. In this way, 70% of the carbon contamination present on the Si standard is also subtracted from the SiC spectrum (Fig. 20). Applying the standardless *Quantex* + / *XPP* quantitative procedure to the resulting SiC spectrum leads to a satisfactory carbon concentration, only ~ 3% relative higher than the nominal one.

Background in Stratified Specimens

In this paragraph, the example of the Cr layer on GaAs substrate will be used to illustrate the problems that may appear in modeling the low-energy background of stratified specimens. First, it should be noted that there is no problem above ~ 600 eV to model the background of a bulk GaAs specimen in the vicinity of the Ga and As L lines. But when AsGa is coated with a ~ 120 nm Cr layer, a significant disagreement between the computed "bremsstrahlung" and the actual spectrum appears in the region between the Ga L and the Cr L lines (Fig. 21). This is due to the strong absorption of the photons having an energy just above the Cr L levels. This absorption is clearly visible on Fig. 22, where the spectra of coated and uncoated GaAs are compared. At the present time, the practical problem is that no routine EDS procedure takes properly into account this absorption phenomena, since all of them perform the computation of the background absorption by assuming that the

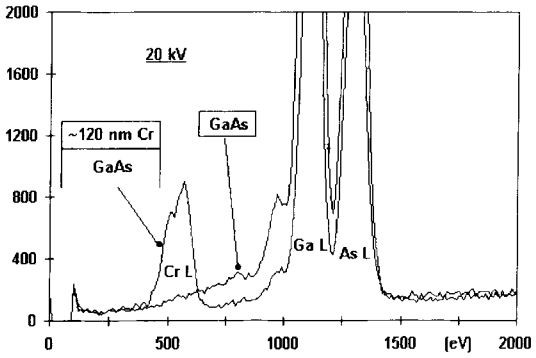

Fig. 22. Comparison of the backgrounds of uncoated and Cr-coated GaAs

elements are homogeneously distributed inside the specimen. Hence, the analyst has to be conscious of the problem that, in the present example, subtracting the background of Fig. 21 would lead to analyze Ga by default compared to As. The other alternative, which would lead to analyze Ga by excess, would be to subtract a linear background by interpolating from the low-energy side of the Ga line to the high-energy side of the As line. By doing so, the "true" value would be somewhere between the two results.

Regarding the background subtraction below the Cr L lines, it can be seen on Fig. 21 that taking a linear interpolation would be better than taking the theoretical "bremsstrahlung".

Conclusions

In the field of material science, and also in other fields (geology, biology,...), there is a growing interest for the microanalysis of ultra-light elements and for the measurement of soft X rays in general. An increasing number of problems require to adopt a "stratified specimen approach", either because of the actual structure of the specimen, or because it has to be coated to avoid charging effects. For applications to layered specimens, the use of soft X rays enables to obtain a reduced depth of ionization. For the microanalysis of multiphase specimens, it also permits to eliminate most of the secondary emission by fluorescence that occurs when lines of higher energy are employed.

A lot of difficulties subsist (contamination, coating, background subtraction, line interference, line distortion, absorption, ...), so that any experiment requires a cautious approach and a real understanding of the physical processes involved.

Acknowledgements. The author acknowledges D. Boivin and Y. Pioche for their contribution to the measurements, most of them specially made for this paper. The development of the program *Strata* and the implementation of the model *XPP* into the *Quantex* software were done in cooperation with SAMx, under contract *ONERA/SAMx* # 6361.

References

[1] J. L. Pouchou, F. Pichoir, *Electron Probe Quantitation*, Plenum, New York, 1991, p. 31.
[2] M. Fialin, G. Remond, C. Bonnelle, *Microbeam Analysis*, VCH, New York, 1994, p. 237.
[3] J. L. Pouchou, F. Pichoir, *J. Microsc. Spectrosc. Electron.* **1986**, *11*, 229.

[4] G. F. Bastin, H. J. M. Heijligers, *Scanning* **1990**, *12*, 225.
[5] J. L. Pouchou, F. Pichoir, *La Recherche Aérospatiale* (English edition), **1984**, *3*, 13.
[6] G. F. Bastin, H. J. M. Heijligers, *X-Ray Spectrometry* **1986**, *15*, 135.
[7] J. L. Pouchou, F. Pichoir, *J. Microsc. Spectrosc. Electron* **1985**, *10*, 291.
[8] J. A. Bearden, *X-Ray Wavelengths*, U.S. Atomic Energy Commission Publ., 1964.
[9] J. L. Pouchou, F. Pichoir, *Microbeam Analysis*, San Francisco Press, San Francisco, p. 319.
[10] K. F. J. Heinrich, *Proc. ICXOM 11*, Univ. Western Ontario Publ., 1987, p. 67.
[11] P. Willich, *Personal Communication*, 1992.
[12] J. L. Pouchou, *Mikrochim. Acta* **1994**, *114/115*, 33.
[13] J. Cazaux, *J. Appl. Phys.* **1986**, *59*, 1418.
[14] J. L. Pouchou, F. Pichoir, *Scanning Microscopy* **1993**, [*Suppl.* 7], 167.
[15] J. L. Pouchou, F. Pichoir, D. Boivin, *Microbeam Analysis*, San Francisco Press, San Francisco, 1990, p. 120.
[16] G. Love, V. D. Scott, A. O. Sandborg, *Microbeam Analysis*, San Francisco Press, San Francisco, 1984, p. 191.